The Role of Porphyrin-to-Porphyrin Linkage Topology in the Extensive Modulation of the Absorptive and Emissive Properties of a Series of Ethynyl- and Butadiynyl-Bridged Bis- and Tris(porphinato)zinc Chromophores

Victor S.-Y. Lin and Michael J. Therien*

Abstract: A new method for the regulation of the photophysical properties of highly conjugated porphyrin arrays is described. The absorptive and emissive signatures of such supramolecular structures can be modulated to an impressive degree by regulation of: i) the extent of the steric interactions that define the barrier to rotation about the conjugated bridge between the porphyrin chromophores, and ii) the magnitude of ground state chromophore–chromophore electronic communication within the supermolecule. The power of this approach is illustrated by the straightforward synthesis as well as the electronic and emission spectra of eight different porphyrin arrays in which (5,10,15,20-tetraphenylporphinato)zinc(II) and (10,20-diphenylporphinato)zinc(II) complexes are joined by ethyne or butadiyne groups. The points of connectivity of these bridges between the chromophoric building blocks are systematically varied to produce a series of supramolecular structures with *meso*-to-*meso*, *meso*-to-β, or β-to-β linkage topologies. These variations allow excellent control of the ground- and excited-state characteristics of the arrays in the series by regulating the degree of both excitonic and electronic porphyrin-to-porphyrin coupling. Our approach shows the precision with which photophysical properties can be engineered in appropriately designed supramolecular systems.

Keywords
conjugation · connectivity · electronic coupling · metalloporphyrins · photosynthesis

Introduction

Owing to the central importance of multichromophoric assemblies based on the porphyrin ring system in biological light harvesting, excitation–migration, and electron transfer,[1, 2] considerable attention has been focused on the elucidation of design requirements for effective biomimetic modeling of the photophysics of natural energy-transducing systems.[3, 4] Fundamental insights into the optimization of specific photophysical properties of multichromophore-containing supermolecules, such as the transition dipole moment, excited-state anisotropy, electronic absorption profile, emission wavelength, and excited-state interchromophore coupling, will not only affect our understanding of biophysical processes such as light harvesting and excitation transfer, but will aid in the development of dyes, sensitizers, optical probes, photonic materials, and optoelectronic devices.

Supramolecular multiporphyrin complexes have been assembled featuring a variety of different porphyrin-to-porphyrin linkages that have included aromatic entities such as *o*-, *m*-, *p*-phenylenes,[5] biphenyls,[6] naphthalenes,[7] anthracenes,[5c, 8] and diphenylacetylenes,[9] as well as aliphatic[10] and vinylic[11] groups. In general, the optical spectra of these systems evince relatively weak chromophore–chromophore excitonic coupling and bear little resemblance to the spectra of biological light-harvesting and excitation-transfer antennae apparatus.[1b, 2] These types of porphyrin arrays contrast sharply with more highly conjugated porphyrin-based supramolecular systems in which ethyne or butadiyne groups join the porphyrin macrocycles directly at their *meso*- or β-carbon positions;[4, 12–14] members of this new class of highly conjugated multichromophoric systems exhibit exceptional ground- and excited-state porphyrin–porphyrin electronic coupling[4, 13] exceeding that observed for face-to-face bis(porphyrin) systems with small porphyrin–porphyrin interplanar separations.[15]

In the present paper we report a straightforward approach that extensively regulates the photophysical properties of such highly conjugated porphyrin arrays. This method relies on modulating the extent of porphyrin–porphyrin steric interactions, which control the torsional barrier to rotation about the conjugated bridge between the constituent chromophores of the assembly and the magnitude of the ground state of chromophore–chromophore electronic coupling within the supermolecule, to effect dramatic, predictable changes of the array's absorptive and emissive signatures. The points of connectivity of the conjugated ethyne or butadiyne bridges between the (porphinato)zinc units are systematically varied to produce a family of supramolecular structures with *meso*-to-*meso*, *meso*-to-β, and β-to-β linkage topologies. We show that these variations in the chromophore–chromophore linkage motif not only allow exquisite control of the photophysical properties of the multiporphyrinic assembly through the regulation of porphyrin–porphyrin excitonic and electronic interactions, but also define a new engineering paradigm in supramolecular photochemistry.

[*] Prof. M. J. Therien, V. S.-Y. Lin
Department of Chemistry, University of Pennsylvania
Philadelphia, Pennsylvania 19104-6323 (USA)
Telefax: Int. code + (215)898-6242

  0947-6539/95/0109-0645 $ 10.00+.25/0

Results and Discussion

The ethyne- and butadiyne-bridged bis- and tris(porphinato)zinc complexes examined in this study, namely, **1**, **2**, **3**[4] (Fig. 1), **4**,[4] **5**, **6** (Fig. 2), **7**, and **8** (Fig. 4),[4] are based upon (5,10,15,20-tetraphenylporphinato)zinc(II) (ZnTPP) and (10,20-diphenylporphinato)zinc(II) (ZnDPP) building blocks. Arrays **1**–**8** were synthesized by metal-mediated cross-coupling reactions utilizing (5-ethynyl-10,20-diphenylporphinato)zinc(II) (**9**),[4] (5,15-diethynyl-10,20-diphenylporphinato)zinc(II) (**10**),[4] (2-ethynyl-5,10,15,20-tetraphenylporphinato)zinc(II) (**11**),[4] and (2,12-diethynyl-5,10,15,20-tetraphenylporphinato)zinc(II) (**12**) with appropriately halogenated (porphinato)zinc precursors.[4, 16, 17]

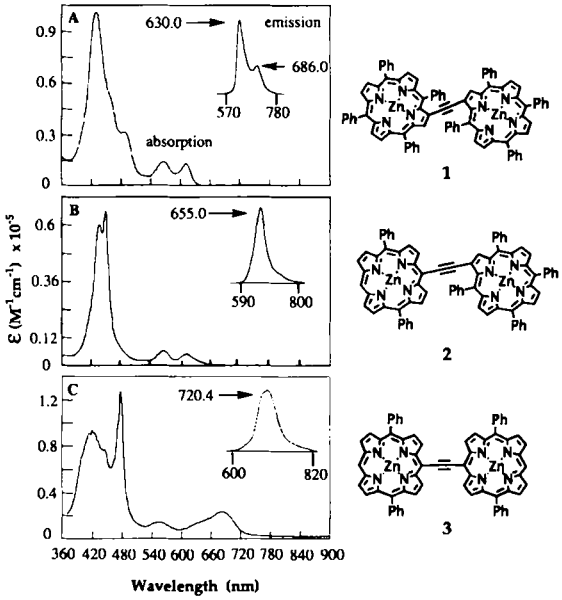

Fig. 1. Room temperature electronic absorption and fluorescence emission spectra of ethyne-bridged bis[(porphinato)zinc] complexes **1**, **2**, and **3** in $CHCl_3$ solution.

Figure 1 shows the electronic absorption and emission spectra of ethynyl-bridged bis[(porphinato)zinc] complexes **1**, **2**, and **3**, which feature respectively *β*-to-*β*, *meso*-to-*β*, and *meso*-to-*meso* linkage topologies between the (porphinato)zinc units. The optical features of these supramolecular chromophoric systems differ remarkably (Table 1). The intense Soret (B) transitions of **1**, **2**, and **3** occurring in the blue region of the spectrum span wavelength ranges of 373–519, 382–508, 360–526 nm, respectively. While previous work has shown that the exciton model can be used to account qualitatively for the spectral splitting in the high-energy visible range,[4] the full width at half maximum (FWHM) of the B-band region can be taken as an approximate measure of the relative extent of (porphinato)zinc–(porphinato)zinc excitonic coupling in the S_2 state (Table 2). Bis[(porphinato)zinc] complexes **1**, **2**, and **3** display high oscillator strength absorptive features in the blue region of the spectrum, in which the FWHM of the B-band regime varies greatly (1699 to 4600 cm^{-1}). Note that the B-band-region spectral breadth of **3**, with a *meso*-to-*meso* linkage, exceeds that of *meso*-to-*β* ethyne-bridged **2** by $\sim 2700\ cm^{-1}$. The absorptive

Table 1. Prominent absorption and emission bands for complexes **1**–**8** recorded in $CHCl_3$.

	Electronic absorption						Fluorescent emission	
	B-band region			Q-band region				
	λ (nm)	ν (cm^{-1})	log(ε)	λ (nm)	ν (cm^{-1})	log(ε)	λ (nm)	ν (cm^{-1})
ZnTPP	427.7	23381	5.78	563.7	17704	4.36	603.0	16584
				605.4	16518	4.09	652.5	15326
ZnDPP	411.7	24290	5.37	540.4	18505	3.94	587.0	17036
							636.0	15723
1	430.2	23245	5.01	566.6	17693	4.15	634.0	15873
	455.9	21937	4.73	611.1	16364	4.13	690.0	14577
	485.6	20369	4.50					
2	432.9	23100	4.78	563.1	17735	3.81	655.0	15267
	445.1	22469	4.82	609.8	16400	3.70		
3 [4]	413.9	24160	4.96	549.2	18208	4.15	720.4	13881
	420.5	23781	4.97	552.5	18100	4.14		
	426.0	23474	4.69	557.8	17928	4.15		
	432.6	23116	4.92	625.1	15997	4.09		
	445.8	22432	4.89	683.4	14633	4.37		
	477.7	20934	5.10					
4 [4]	438.1	22826	4.64	569.5	17559	3.80	621.1	16100
	460.1	21734	4.44	611.9	16343	3.76	671.2	14899
	489.8	20417	4.16					
5	430.2	23172	5.07	566.6	17651	4.20	647.5	15444
	450.5	22201	5.01	640.8	15606	4.47		
	474.8	21064	4.79					
6	422.1	23691	4.93	562.5	17821	4.16	688.5	14524
	446.4	22401	5.07	627.3	15941	4.27		
	478.8	20886	4.79	675.9	14795	4.34		
7	431.6	23172	4.87	562.5	17735	4.07	634.0	15773
	473.4	21124	4.58	625.9	15975	4.16	700.0	14286
	490.9	20369	4.50					
8 [4], [a]	420.5	23781	4.84	552.0	18116	3.99	835.5	11969
	437.0	22883	4.72	802.2	12466	4.63		
	457.2	21872	4.66					
	464.5	21529	4.66					
	490.9	20371	4.85					
	500.8	19968	4.95					

[a] Recorded in 10:1 $CHCl_3$:pyridine.

0947-6539/95/0109-0646 $ 10.00+.25/0 Chem. Eur. J. 1995, 1, No. 9

Table 2. Comparative integrated oscillator strengths (OS) and absorptive domains of the blue and red spectral regions of complexes **1**–**8**.

	FWHM [a] [cm^{-1}] B-band region	OS [b] B-band region	FWHM [c] [cm^{-1}, (nm)] Q-band region		OS [d] Q-band region	OS 360–900 nm
ZnTPP	696	0.882	841 657	(563.7) (605.4)	0.129	1.011
ZnDPP	783	0.864	792	(540.4)	0.035	0.899
1	2569	1.607	1308 997	(566.6) (611.1)	0.121	1.728
2	1699	0.836	1070 1129	(563.1) (609.8)	0.083	0.919
3	4600	2.234	2385 2009	(549.2) (683.4)	0.358	2.592
4	3000	1.390	1261 916	(569.5) (611.9)	0.139	1.529
5	3647	1.929	1873 1013	(566.6) (640.8)	0.231	2.160
6	4686	1.862	1749 2044	(562.5) (675.9)	0.298	2.160
7	3508	1.388	1727 945	(562.5) (626.0)	0.185	1.573
8	4995	1.810	1485	(802.2)	0.452	2.262

[a] Taken as the spectral width of the B-band region at half the height of the most intense absorption. [b] Oscillator strengths calculated over the following wavelength domains: **1**, 360–529 nm; **2**, 360–517 nm; **3**, 360–523 nm; **4**, 360–528 nm; **5**, 360–530 nm; **6**, 360–519 nm; **7**, 360–534 nm; **8**, 360–540 nm. [c] Entries correspond to the spectral window centered about the electronic transiton in parentheses. See Figures 1, 2, and 4. [d] Oscillator strengths calculated over the following wavelength domains: **1**, 529–900 nm; **2**, 517–900 nm; **3**, 523–900 nm; **4**, 528–900 nm; **5**, 530–900 nm; **6**, 519–900 nm; **7**, 534–900 nm; **8**, 540–900 nm.

features in the Q-band region show similar diversity, with the lowest-energy Q-type transitions of **1**, **2**, and **3** spanning a $\sim 1490\ cm^{-1}$ domain (Table 1). Since the energy of the lowest-energy Q-type transition is a measure of the $\pi-\pi^*$ gap and hence of the degree of porphyrin–porphyrin conjugative interactions in the ground state, Figure 1 demonstrates that the magnitudes of both excitonic and electronic coupling depend intimately on the mode of porphyrin–porphyrin connectivity.

Figure 2 depicts the absorption and emission profiles of molecules **4**, **5**, and **6**, the butadiynyl bridge analogues of complexes **1**, **2**, and **3**. The (porphinato)zinc arrays **4**, **5**, and **6** exhibit B-band-region absorptions that span a near-constant window of the solar spectrum (372–522 nm), though the FWHMs of their respective Soret regions vary over approximately

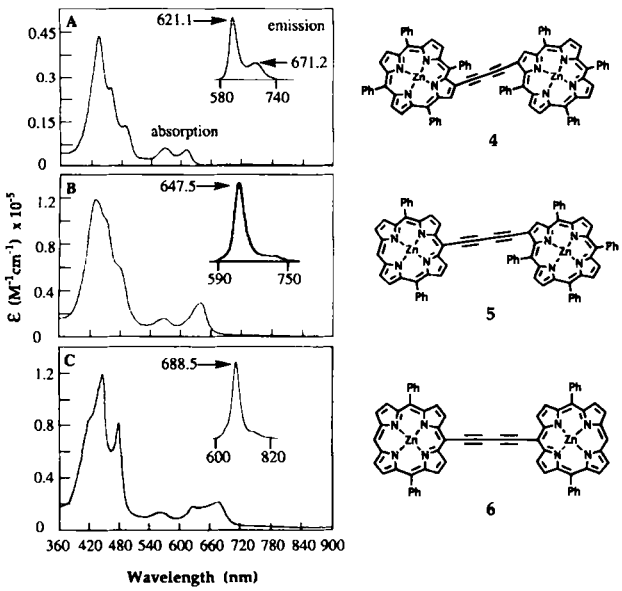

Fig. 2. Room temperature electronic absorption and fluorescence emission spectra of butadiyne-bridged bis[(porphinato)zinc] complexes **4**, **5**, and **6** in $CHCl_3$ solution.

$1700\ cm^{-1}$ and are strongly dependent on the nature of porphyrin-to-porphyrin connectivity (Table 2). The wavelength of the lowest-energy $\pi-\pi^*$ transition displays a similar relationship to butadiynyl bridging topology: altering the mode of connectivity for the butadiyne from β-to-β to *meso*-to-β to *meso*-to-*meso* results in a shift of the lowest-energy Q-type transition from 611.9 to 640.8 to 675.9 nm; this demonstrates predictable absorptive modulation over a $1550\ cm^{-1}$ frequency domain. The butadiyne-bridged bis[(porphinato)zinc] series shows that the magnitudes of both excitonic and electronic coupling in these systems exhibit the same dependence on porphyrin–porphyrin connectivity, with *meso*-to-*meso* > *meso*-to-β > β-to-β; this contrasts with the behavior of their ethyne-bridged analogues, in which the degree of excitonic coupling in the supramolecular systems follows the order *meso*-to-*meso* > β-to-β > *meso*-to-β while the relative magnitudes of porphyrin–porphyrin conjugative interactions are *meso*-to-*meso* > *meso*-to-$\beta \geq \beta$-to-β.

Although the large excitonic splittings derive in part from the close interspatial separation of the chromophoric (porphinato)zinc units and the fact that the ZnDPP and ZnTPP components of the arrays have enormous associated transition dipole moments, the large electronic coupling between the porphyrin macrocycles permitted by the ethyne and butadiyne bridges is chiefly responsible for the dramatically enhanced excitonic interactions in these species. While a complete theoretical analysis of the electronic spectra of conjugated bis[(porphinato)zinc] chromophores **1**–**6** will be presented elsewhere,[18] Figure 3 provides some insight into the origin of the disparate optical absorption profiles. The dihedral-angle-dependent energy maps of complexes **1**–**6** were obtained using MOPAC 6.0.[19] Although these calculations may underestimate the degree of electronic stabilization of coplanar bis(chromophore) geometries, especially for arrays with the *meso*-to-*meso* linkage topology (possibly due to not accounting for a small degree of charge resonance character in the ground states of these systems),[20–21] a number of conclusions can be drawn from this study. For example, the calculations predict that the integral ZnDPP and ZnTPP chromophores of *meso*-to-β ethyne-bridged

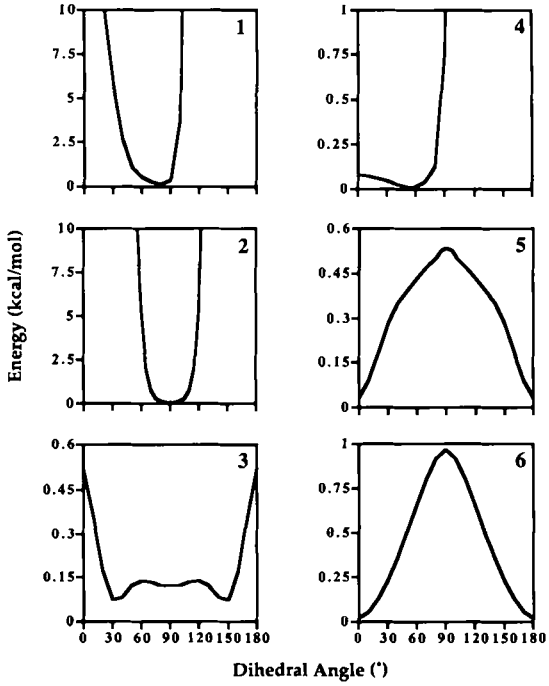

Fig. 3. Porphyrin–porphyrin dihedral-angle-dependent energy maps of ethyne- and butadiyne-bridged bis[(porphinato)zinc] complexes **1**–**6**. The calculated conformational energies correspond to heats of formation (kcal mol^{-1}) determined using CAChe MOPAC 6.0 with standard AM 1 semiempirical Hamiltonian parameterization. Internal coordinates were optimized at each geometry; potential energy maps are unsmoothed and generated by straight line connectivity of the evaluated heats of formation determined every 10°.

2 will exist in an orthogonal conformation. Interestingly, Figure 1 and Table 2 indicate that the electronic spectrum of **2** cannot be approximated by a simple superposition of the ZnDPP and ZnTPP optical spectra, as: i) the FWHM of **2**'s B-band region exceeds the sum of its two component (porphinato)zinc building blocks by 220 cm^{-1}; and ii) the lowest-energy Q band maximum of **2** is red-shifted by 154 cm^{-1} relative to the Q(0,0) transition of ZnTPP, and tails further out to the red. Thus, even for this extreme chromophore–chromophore geometry, exciton splitting of the S_2 state is observed and the magnitude of the π–π^* gap of **2** is influenced by the small but detectable porphyrin–porphyrin electronic coupling. While this latter effect probably derives from the libration of the ZnDPP and ZnTPP subunits about the *meso*-to-β ethyne bridge possible at room temperature, it is nevertheless crucial to recognize that **2**'s optical properties contrast markedly with ethynyl- and butadiynyl-bridged bis[(porphinato)zinc] complexes **1**, **3**, **4**, **5**, and **6**. This underscores the degree to which restriction of chromophore–chromophore torsional motion about a bridge of minimal length, even about one that possesses π cylindrical symmetry, can affect the optical properties of the supramolecular system; this is particularly evident when the electronic spectrum of **2** is viewed alongside that of **5**, which we predict will possess only a small barrier to rotation about the butadiyne bridge and a minimum-energy coplanar bis[(porphinato)zinc] arrangement.

The calculated energy versus chromophore–chromophore dihedral angle plots of compounds **1**–**6** allow us to estimate the effect that the mode of connectivity has upon the electronic properties of a given supramolecular system. Molecules **3**, **5**, and **6** all possess barriers to one complete revolution about their respective conjugated bridges of less than 1 kcal mol^{-1} (Fig. 3). Figures 1 and 2, along with Table 1, show that the energy of the lowest-energy Q-type transition for these compounds decreases in the order **5** > **6** > **3**; moreover, the fluorescent emission energy in these complexes follows the same trend and varies considerably (**5**, 15444 cm^{-1}; **6**, 14524 cm^{-1}; **3**, 13881 cm^{-1}). These trends in the optical and emission spectra derive from the magnitude of the π–π^* gap; thus they indicate that (porphinato)zinc–(porphinato)zinc electronic coupling increases in the order **5** < **6** < **3**. These chromophores will all have approximately similar relative distributions of (porphinato)zinc–(porphinato)zinc geometries at room temperature; since both compounds **5** and **6** have butadiynyl bridges, these calculations indicate that *meso*-to-*meso* connectivity affords superior porphyrin–porphyrin electronic coupling with respect to *meso*-to-β conjugated bridges for a set chromophore–chromophore torsional angle.

Evidence suggesting that *meso*-to-β connectivity similarly provides enhanced electronic coupling with respect to the β-to-β linkage can also be gleaned from Figure 3. Here β-to-β ethyne-bridged **1** and *meso*-to-β ethyne-bridged **2** have calculated minimum energy torsional angles of 80° and 90°, respectively; for both of these complexes, these porphyrin–porphyrin geometries have similarly nested minima with equally substantial rotational barriers to molecular configurations lying higher than their respective minimum energy conformations. While both **1** and **2** exhibit Q-type absorptions of similar energy to the Q(0,0) and Q(1,0) transitions of ZnTPP, signaling that both these ethyne-bridged arrays have essentially electronically decoupled ground states, we would expect that if the (porphinato)zinc–(porphinato)zinc dihedral angle was the only determinant of electronic coupling, then compound **1** would have the smaller π–π^* gap and the redder emission wavelength. That the π–π^* gaps of **1** and **2** are virtually identical, with **2** displaying the lower-energy emission maximum, emphasizes the importance of porphyrin-to-porphyrin linkage topology in determining the photophysical properties of these highly conjugated porphyrin arrays. This conclusion agrees with the predictions of simple molecular orbital calculations for porphine, which show a significantly greater electron density at the porphyrin *meso* positions than the β for both the HOMO and LUMO.[22]

Figure 3, together with the spectra displayed in Figures 1 and 2, stresses the significance of the length of the conjugated bridge in determining the magnitude of ground- and excited-state electronic interactions. The *meso*-to-*meso* linked systems **3** and **6** have virtually identical barriers to a 180° rotation about their respective conjugated bridges, yet the π–π^* gap in **3** is 162 cm^{-1} smaller, demonstrating that the butadiyne bridge mediates porphyrin–porphyrin electronic coupling less efficiently than an ethyne moiety. A similar conclusion can be drawn from the data presented for β-to-β linked compounds **1** and **4**. Although our MOPAC calculations show that substantial steric barriers to rotation are present in both these compounds, the dihedral angle energy maps for these species are quite different. While rotation of the ZnTPP components of **4** beyond 90° is prohibited, these calculations reveal that a much shallower potential energy surface exists between ±85°, with minima occurring at ±55°; moreover, only a small barrier is predicted for the attainment of a geometry in which the ZnTPP units of **4** are coplanar: this contrasts with **1**, in which the dihedral angle between the ZnTPP components is essentially locked at 80°. Since the low-energy visible regions of the spectra of **1** and **4** are quite similar, and the molecular conformations attainable by **4** at room temperature would favor increased conjugation, we are forced to conclude that any enhanced coupling in **4** facilitated by the relative geometry of its ZnTPP–ZnTPP units is negated by decreased porphyrin–porphyrin electronic communication caused by the butadiynyl bridging moiety.

0947-6539/95/0109-0648 $ 10.00+.25/0 Chem. Eur. J. 1995, 1, No. 9

In sum, Figure 3 suggests that for the case of butadiyne-bridged bis[(porphinato)zinc] systems **4**–**6**, which might be expected to have nearly equal propensities to attain a coplanar bis(porphyrin) arrangement at high temperature, the wavelengths of the low-energy absorption bands are determined primarily by the relative degrees of porphyrin–porphyrin coupling afforded by the three linkage motifs; for these complexes the magnitude of excitonic coupling is related to the extent of chromophore–chromophore conjugative interactions (*meso*-to-*meso* > *meso*-to-β > β-to-β) while the B-band splitting pattern is dominated by the relative spatial arrangement of the *x*- and *y*-polarized transition dipoles on the individual (porphinato)zinc units. For ethyne-bridged (porphinato)zinc arrays **1**–**3**, only the most strongly coupled bis[(porphinato)zinc] chromophore, **3**, demonstrates impressive excitonic splitting and a dramatic red shift of the lowest-energy transition. The precipitous drop in ground-state coupling from **3** to **2** and **1** originates in the poor conjugative interactions enforced by the large (porphinato)zinc–(porphinato)zinc dihedral angles in these systems; this essentially masks most of the spectral effects that derive from the differences in electronic communication afforded by the three different bridging motifs.

Table 2 shows that a similar dependence of the integrated oscillator strength of the B- and Q-band regions on the relative degree of porphyrin–porphyrin coupling exists. While compounds **1**–**6** all possess high extinction-coefficient transitions in both the blue and red regions of the spectrum, the magnitude of the oscillator strength in these spectral regions correlates in general with the extent of porphyrin–porphyrin conjugation in the respective bis[(porphinato)zinc] systems. It is interesting to note that *meso*-to-β ethyne-bridged **2** is the one exception to this observation, and actually exhibits a significant drop in integrated oscillator strength in both the B- and Q-band regions relative to compound **1**, which possesses β-to-β ethynyl connectivity, despite the very minor differences in relative porphyrin-to-porphyrin electronic communication between these two supramolecular systems. While all modes of porphyrin–porphyrin linkage topology exhibited by compounds **1**, **3**, **4**, **5**, and **6** lead to an increase in oscillator strength in the B-band region with respect to ZnDPP and ZnTPP, only *meso*-to-β and *meso*-to-*meso* connectivities lead to significant oscillator-strength enhancements in the red region of the spectrum.

The emission spectra of compounds **1**–**6** (insets, Figs. 1 and 2) show that all of the bis[(porphinato)zinc] chromophores save **2** display relatively small Stokes shifts (162–752 cm^{-1}).[23] The magnitude of the Stokes shift decreases with increasing length of the conjugated bridge for a constant mode of porphyrin-to-porphyrin connectivity. Most interesting, of course, is the astonishing control that linkage topology exerts over the wavelength of the emission maximum; note that compounds **4**, **1**, **5**, **2**, **6**, and **3** emit strongly at 621.1, 630.0, 647.5, 655.0, 688.5, and 720.4 nm, respectively. Altering the nature of the conjugated bridge from butadiyne to ethyne while varying the porphyrin–porphyrin bridge from β-to-β to *meso*-to-β to *meso*-to-*meso* thus effects significant and predictable tuning of the emission maxima of conjugated porphyrin arrays **1**–**6** that span a 2200 cm^{-1} frequency range.

Figure 4 highlights the extent of absorptive and emissive modulation possible in an analogous series of conjugated tris[(porphinato)zinc] arrays. Although the excitonic splitting patterns of **7** and **8** are similar to their respective bis[(porphinato)zinc] structural analogues **4** and **3**, a distinct increase in the FWHM of their B-band regions has occurred: **7**, in which two butadiynyl groups link two ZnTPP units to a central ZnTPP moiety at its 2- and 12-positions, possesses a FWHM of approximately 3500 cm^{-1}, and **8**, in which two ethyne moieties connect the three (5,15-diphenylporphinato)zinc macrocycles at their respective *meso*-carbon positions, has a FWHM of nearly 5000 cm^{-1} (Table 2). Figure 4 suggests that considerable control can be exerted over photophysical properties, such as the wavelengths of low energy absorption and fluorescence emission bands, that derive from the magnitude of the supramolecular chromophore π–π^* gap in higher-order arrays based on the linkage types illustrated in Figures 1 and 2. Thus compounds **7** and **8** clearly demonstrate that the frequency of the lowest-energy absorption can be predictably varied over a 3510 cm^{-1} range while the emission maximum of the supramolecular chromophore can be tuned over a 3800 cm^{-1} spectral window (Table 1) for an analogous series of *meso*-to-*meso*, *meso*-to-β, and β-to-β ethyne- and butadiyne-bridged tris[(porphinato)zinc] chromophores.

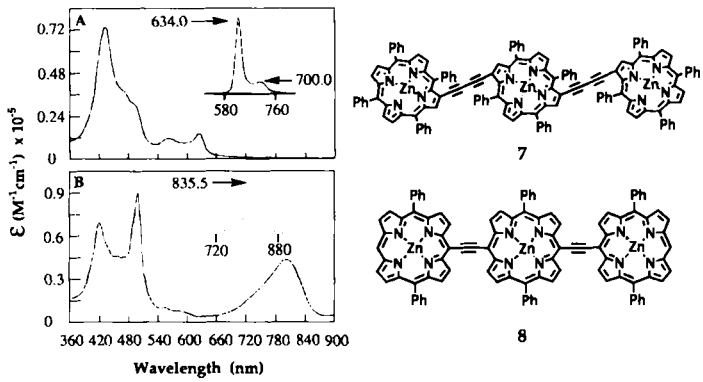

Fig. 4. Electronic absorption and fluorescence emission spectra of conjugated tris[(porphinato)zinc] arrays **7** and **8** at room temperature. (**A**) β-to-β butadiyne-bridged **7** in $CHCl_3$; (**B**) *meso*-to-*meso* ethyne-bridged **8** in 10:1 $CHCl_3$:pyridine.

Summary and Conclusion

All of these ethyne- and butadiyne-bridged porphyrin arrays exhibit extraordinarily large excitonic coupling in the S_2 excited singlet state, greatly exceeding that observed for all other porphyrin-to-porphyrin linkage topologies that have hitherto been utilized for assembling supramolecular multiporphyrinic systems. In general, we find that the degree of porphyrin–porphyrin electronic coupling decreases with increasing bridge length for a specific linkage topology; most importantly, the magnitude of this coupling is extremely sensitive to the connection sites of the ethynyl or butadiynyl interchromophore bridges on the porphyrin carbon framework. The electronic coupling can be further attenuated for a specific conjugated bridge length when severely disparate steric interactions exist for the three types of porphyrin-to-porphyrin linkage and enforce non-isostructural (porphinato)zinc–(porphinato)zinc orientations or distributions of orientations for the supramolecular systems, as was observed for the ethyne-bridged bis[(porphinato)zinc] molecules **1**, **2**, and **3**. When such steric effects are not manifest, the magnitude of electronic coupling between the porphyrinic components of the array depends strictly upon the porphyrin-to-porphyrin bridge type and follows the order *meso*-to-*meso* > *meso*-to-β > β-to-β. Other photophysical properties of these arrays, such as the degree of red shift of the Q-type absorptions, the magnitude of the oscillator strength of these absorptions, and the wavelength of their emission maximum, correlate likewise with linkage topology. For all these conjugated porphyrin arrays, the salient features of the actual B-band splitting

  0947-6539/95/0109-0649 $ 10.00+.25/0

pattern is a function of the relative orientations of the *x*- and *y*-polarized ZnDPP- and ZnTPP-localized transition dipoles and can be explained by the point-dipole coupling models described by Kasha.[24]

While no other chromophore–chromophore bridging unit enables such varied control of supramolecular absorptive characteristics and photophysical properties, it is important to recognize that the unusual breadth of absorptive and emissive regulation provided by this family of ethynyl- and butadiynyl-bridged (porphinato)zinc arrays has been attained without extensive derivatization of the macrocycle periphery of the constituent chromophoric building blocks. The magnitude of the spectral modulation attainable with these systems far exceeds the type of fine-tuning possible through derivatization of a single porphyrin chromophore. Moreover, the fact that an enormous number of conjugated porphyrin arrays can be accessed from a few ethyne-elaborated monomeric porphyrins underscores the potential of this approach to engineer precisely the photophysical properties of multichromophoric assemblies. Finally, with respect to elucidating key design requirements in the area of supramolecular photochemistry, this series of ethynyl- and butadiynyl-bridged bis- and tris(porphinato)zinc compounds defines a basis set of supramolecular chromophore systems in which to examine ultrafast electron and excitation transfer processes at high donor–acceptor electronic coupling, as well as to explore how the relative degrees of excitonic and electronic interactions affect photophysical properties relevant to biomimetic photosynthetic energy transduction, such as excited-state lifetime, anisotropy, and spin alignment.

Experimental Procedure

The syntheses of porphyrin arrays **3**, **4**, and **8** from their ethyne-elaborated porphyrinic building blocks **9**, **10**, and **11** have been reported earlier.[4] Construction of **1**, **2**, **5**, **6**, **7**, and **12** utilize previously established methodology;[4, 16] experimental details and characterization data for these complexes are outlined below. Temperature-dependent spectroscopic studies focusing on the dynamical properties of these compounds will be reported separately.[25]

Bis[(2,2′-5,10,15,20-tetraphenylporphinato)zinc(II)]ethyne (**1**): $Pd(PPh_3)_4$ (20 mg, 0.0173 mmol) and CuI (10 mg) were added to a solution of (2-bromo-5,10,15,20-tetraphenylporphinato)zinc(II) (228 mg, 0.3 mmol) in THF (20 mL). (2-ethynyl-5,10,15,20-tetraphenylporphinato)zinc(II) (147 mg, 0.21 mmol) and diethylamine (0.35 mL) in THF (20 mL) were added to this solution by canula. After being stirred under N_2 at 50 °C for 24 h, the mixture was separated by column chromatography on silica with hexanes:THF (7:3) as eluant. The first reddish-green band ($R_f \approx 0.3$) running after the band of unreacted starting material was isolated and crystallized to give the product (yield = 56% based on the (2-ethynyl-5,10,15,20-tetraphenylporphinato)zinc(II) starting material). Selected characterization data: ^{1}H NMR (250 MHz, $CDCl_3$): δ = 9.26 (s, 2H), 8.89 (m, 12H), 8.27 (m, 4H), 8.20 (m, 12H), 7.97 (m, 4H), 7.83 (m, 2H), 7.75 (m, 18H); Vis ($CHCl_3$): see Table 1. FAB MS: 1374 (calcd 1374).

{[(2-5,10,15,20-Tetraphenylporphinato)zinc(II)]-[5′-10′,20′-diphenylporphinato)-zinc(II)]}ethyne (**2**): $Pd(PPh_3)_4$ (20 mg, 0.0173 mmol) and CuI (10 mg) were added to a solution of (5-bromo-10,20-diphenylporphinato)zinc(II) (126 mg, 0.21 mmol) in THF (20 mL). (2-Ethynyl-5,10,15,20-tetraphenylporphinato)zinc(II) (150 mg, 0.21 mmol) and diethylamine (0.35 mL) in THF (20 mL) were added to this solution by canula. The solution was stirred under N_2 for 12 h. The product was isolated and purified by column chromatography on silica using hexanes:THF (4:1) as eluant. A brown-green band was collected and evaporated to yield 200 mg of product (78% yield, based on the porphyrin starting material). Selected characterization data: ^{1}H NMR (250 MHz, $CDCl_3$): δ = 10.16 (s, 1H), 9.72 (d, 2H, J = 4.8 Hz), 9.62 (s, 1H), 9.32 (d, 2H, J = 4.4 Hz), 9.02 (d, 2H, J = 4.5 Hz), 8.97 (m, 6H), 8.87 (d, 1H, J = 4.7 Hz), 8.81 (d, 1H, J = 4.9 Hz), 8.28 (m, 12H), 7.76 (m, 15H), 6.98 (t, 2H, J = 7.7 Hz), 5.93 (t, 1H, J = 7.8 Hz); Vis ($CHCl_3$): see Table 1. FAB MS: 1222 (calcd 1222).

{[(2-5,10,15,20-Tetraphenylporphinato)zinc(II)]-[5′-10′,20′-diphenylporphinato)-zinc(II)]}butadiyne (**5**): Methyl lithium with lithium bromide (1.5 M in diethylether) (0.6 mL, 1 mmol) was added to a solution of 1,4-bis(trimethylsilyl)butadiyne (194.43 mg, 1 mmol) in THF at room temperature. After stirring for 3 h, excess zinc chloride was added to the solution to yield 4-trimethylsilylbutadiynylzinc chloride, which was transferred immediately to a solution of (2-bromo-5,10,15,20-tetraphenylporphinato)zinc(II) (75.9 mg, 0.1 mmol) and $Pd(PPh_3)_4$ (10 mg) in THF (20 mL). After completion of the metal-mediated cross-coupling reaction, chromatography was carried out on silica by using hexanes:THF (9:1) as eluent. The first band was isolated and evaporated to yield (2-trimethylsilylbutadiynyl-5,10,15,20-tetraphenylporphinato)zinc(II) (90% yield, based on the porphyrin starting material). The product was then desilylated, recrystallized, and added to a solution of (5-bromo-10,20-diphenylporphinato)zinc(II) (60 mg, 0.1 mmol) and 10 mg of $Pd(PPh_3)_4$ in THF (20 mL). After stirring at 60 °C for 12 h, the product was purified by chromatography on silica by using hexanes:THF (4:1) as eluent. The first green band was isolated and evaporated to yield 76.3 mg of the product (yield = 61%, based on (5-bromo-10,20-diphenylporphinato)zinc(II)). ^{1}H NMR (500 MHz, $CDCl_3$): δ = 10.04 (s, 1H), 9.77 (d, 2H, J = 4.5 Hz), 9.33 (s, 1H), 9.20 (d, 2H, J = 4.2 Hz), 9.01 (d, 2H, J = 4.5 Hz), 8.89 (d, 2H, J = 4.4 Hz), 8.79 (m, 6H), 8.28 (d, 1H, J = 7.6 Hz), 8.14 (m, 10H), 7.95 (t, 2H, J = 7.6 Hz), 7.81 (t, 1H, J = 7.5 Hz), 7.76 (m, 15H); Vis ($CHCl_3$): see Table 1. FAB MS: 1246 (calcd 1246).

Bis[(5,5′-10,20-diphenylporphinato)zinc(II)]butadiyne (**6**): An oven-dried 50 mL Schlenk tube equipped with a magnetic stirring bar was charged with (5-ethynyl-10,20-diphenylporphinato)zinc(II) (110 mg, 0.2 mmol) and prepurified pyridine (1.4 mL). The solution was stirred under N_2 for 10 min. $Cu(OAc)_2$ (40 mg, 0.2 mmol) in pyridine (2 mL) was heated to 60 °C and added to the porphyrin–pyridine solution by syringe; the mixture was then warmed and stirred at 90 °C for 1 hour. The solution was quenched with H_2O. A crude dark green precipitate was collected, redissolved in THF, dried over $CaCl_2$, and purified by column chromatography on silica using hexanes:THF (7:3) as eluant. A dark green band was collected and evaporated to yield 81.2 mg of product (74% yield, based on the porphyrin starting material). Selected characterization data: ^{1}H NMR (250 MHz, $CDCl_3$): d 10.1 (s, 2H), 9.97 (d, 4H, J = 4.6 Hz), 9.26 (d, 4H, J = 4.0 Hz), 9.01 (d, 4H, J = 4.5 Hz), 8.92 (d, 4H, J = 4.1 Hz), 8.23 (m, 8H), 7.77 (m, 12H); Vis ($CHCl_3$): see Table 1. FAB MS: 1095 (calcd 1095).

2,12-Bis{[(2′-5′,10′,15′,20′-tetraphenylporphinato)zinc(II)]butadiynyl}(5,10,15,20-tetraphenylporphinato)zinc(II) (**7**): A solution of (2,12-diethynyl-5,10,15,20-tetraphenylporphinato)zinc(II) (desilylated **12**; 73 mg, 0.1 mmol), (2-ethynyl-5,10,15,20-tetraphenylporphinato)zinc(II) (desilylated **11**; 140 mg, 0.2 mmol), and prepurified pyridine (1.4 mL) was stirred under N_2 for 10 min. $Cu(OAc)_2$ (20 mg, 0.1 mmol) in pyridine (2 mL) was heated to 60 °C and added to the porphyrin–pyridine solution by syringe; the mixture was then warmed and stirred at 90 °C for 6 h. The solution was quenched with H_2O. A crude dark green precipitate was collected, redissolved in THF, dried over $CaCl_2$, and purified by column chromatography on silica using hexanes:THF (7:3) as eluant. The second dark green band was collected and evaporated to yield 97.8 mg of product (46% yield, based on the (2,12-diethynyl-5,10,15,20-tetraphenylporphinato)zinc(II) starting material). Selected characterization data: ^{1}H NMR (250 MHz, $CDCl_3$): 9.18 (m, 6H), 8.90 (m, 16H), 8.19 (m, 24H), 7.76 (m, 36H); Vis ($CHCl_3$): see Table 1. FAB MS: 2120 (calcd 2120).

(2,12-Diethynyl-5,10,15,20-tetraphenylporphinato)zinc(II) (**12**): A tenfold molar excess of the trimethylsilylethynylzinc chloride was treated with a mixture (difficult to separate) of mono- and di-substituted (*β*-bromo-5,10,15,20-tetraphenylporphinato)zinc complexes in the presence of a catalytic amount of $Pd(PPh_3)_4$ in THF. The products of the cross-coupling reaction were isolated and desilylated to give the corresponding ethynyl- and diethynyl-substituted porphyrins. (2,12-diethynyl-5,10,15,20-tetraphenylporphinato)zinc(II) (**12**) was then purified and separated from other *β*-ethynyl porphyrins by column chromatography on silica gel using hexanes:THF (9:1) as eluent. The second brownish-red band was collected and evaporated. Isolated yield = 89.3 mg ($\approx$ 51.5%, based on 200 mg of the halogenated porphyrin starting material). Selected characterization data: ^{1}H NMR (250 MHz, $CDCl_3$): δ = 9.17 (s, 2H), 8.86 (t, 6H, J = 9.5 Hz), 8.15 (d, 4H, J = 7.4 Hz), 8.05 (d, 4H, J = 7.4 Hz), 7.72 (m, 6H), 7.62 (t, 6H, J = 7.4 Hz), 3.27 (s, 2H); Vis ($CHCl_3$): see Table 1. Elemental analysis (Anal.): Calcd for $C_{48}H_{28}N_4Zn$: C 79.39; H 3.89; N 7.71. Found: C 79.23; H 4.20; N 7.31.

Acknowledgements: This work was supported in part by the National Science Foundation MRL Program (DMR-91-20668). M. J. T. gratefully acknowledges the Searle Scholars Program (Chicago Community Trust), the Arnold and Mabel Beckman Foundation, E. I. du Pont de Nemours, and the National Science Foundation for Young Investigator Awards, as well as the Alfred P. Sloan Foundation for a research fellowship.

Received: July 21, 1995 [F216]

[1] a) J. P. Allen, G. Feher, T. O. Yeates, D. C. Rees, J. Deisenhofer, H. Michel, R. Huber, *Proc. Natl. Acad. Sci. USA* **1986**, *83*, 8589–8593. b) G. McDermott, S. M. Prince, A. A. Freer, A. M. Hawthornthwaite-Lawless, M. Z. Papiz, R. J. Cogdell, N. W. Isaacs, *Nature (London)* **1995**, *374*, 517–521.

[2] R. van Grondelle, J. P. Dekker, T. Gillbro, V. Sundstrom, *Biochim. Biophys. Acta.* **1994**, *1187*, 1–65.

[3] a) M. R. Wasielewski, *Chem. Rev.* **1992**, *92*, 435–461. b) M. P. O'Neil, M. P. Niemczyk, W. A. Svec, D. Gosztola, G. L. Gaines III, M. R. Wasielewski, *Science* **1992**, *257*, 63–65. c) D. Gust, T. A. Moore, A. L. Moore, *Acc. Chem. Res.*

1993, *26*, 198–205. d) S. Anderson, H. L. Anderson, J. K. M. Sanders, *ibid.* **1993**, *26*, 469–475. e) J. L. Sessler, V. L. Capuano, A. Harriman, *J. Am. Chem. Soc.* **1993**, *115*, 4618–4628. f) M. Ohkohchi, A. Takahashi, N. Mataga, T. Okada, A. Osuka, H. Yamada, K. Maruyama, *ibid.* **1993**, *115*, 12137–12143.

[4] V. S.-Y. Lin, S. G. DiMagno, M. J. Therien, *Science* **1994**, *264*, 1105–1111.

[5] a) J. L. Sessler, J. Hugdall, M. R. Johnson, *J. Org. Chem.* **1986**, *51*, 2838–2840. b) J. L. Sessler, M. R. Johnson, T.-Y. Lin, S. E. Creager, *J. Am. Chem. Soc.* **1988**, *110*, 3659–3661. c) T. Nagata, A. Osuka, K. Maruyama, *ibid.* **1990**, *112*, 3054–3059. d) A. Osuka, S. Nakajima, T. Nagata, K. Muruyama, K. Toriumi, *Angew. Chem.* **1991**, *103*, 579; *Angew. Chem. Int. Ed. Engl.* **1991**, *30*, 582–584.

[6] A. Helms, D. Heiler, G. McLendon, *J. Am. Chem. Soc.* **1991**, *113*, 4325–4327.

[7] A. Osuka, K. Maruyama, *J. Am. Chem. Soc.* **1988**, *110*, 4454–4456.

[8] C. K. Chang, I. Abdalmuhdi, *J. Org. Chem.* **1983**, *48*, 5388–5390.

[9] a) S. Prathapan, T. E. Johnson, J. S. Lindsey, *J. Am. Chem. Soc.* **1993**, *115*, 7519–7520. b) R. W. Wagner, J. S. Lindsey, *J. Am. Chem. Soc.* **1994**, *116*, 9759–9760.

[10] a) R. Selensky, D. Holten, M. W. Windsor, J. B. Paine III, D. Dolphin, *Chem. Phys.* **1981**, *60*, 33–46. b) H. Kamogawa, S. Miyama, S. Minoura, *Macromolecules* **1989**, *22*, 2123–2126. c) E. B. Fleischer, A. M. Shachter, *J. Heterocycl. Chem.* **1991**, *28*, 1693–1699. d) E. Scamporrino, D. Vitalini, *Macromolecules* **1992**, *25*, 1625–1632.

[11] a) M. Graça, H. Vicente, K. M. Smith, *J. Org. Chem.* **1991**, *56*, 4407–4418. b) A. K. Burrelll, D. L. Officer, D. C. W. Reid, *Angew. Chem.* **1995**, *107*, 986; *Angew. Chem. Int. Ed. Engl.* **1995**, *34*, 900–902.

[12] a) D. P. Arnold, L. J. Nitschinsk, *Tetrahedron* **1992**, *48*, 8781–8792. b) D. P. Arnold, G. A. Heath, *J. Am. Chem. Soc.* **1993**, *115*, 12197–12198.

[13] a) H. L. Anderson, S. J. Martin, D. D. C. Bradley, *Angew. Chem.* **1994**, *106*, 711; *Angew. Chem. Int. Ed. Engl.* **1994**, *33*, 655–657. b) H. L. Anderson, *Inorg. Chem.* **1994**, *33*, 972–981.

[14] a) P. J. Angiolillo, V. S.-Y. Lin, J. M. Vanderkoii, M. J. Therien, *J. Am. Chem. Soc.*, in press. b) V. S.-Y. Lin, S. A. Williams, M. J. Therien, unpublished results.

[15] a) J. P. Collman, F. C. Anson, C. E. Barnes, S. C. Bencosme, T. Geiger, E. R. Evitt, R. P. Kreh, K. Meier, R. B. Pettman, *J. Am. Chem. Soc.* **1983**, *105*, 2694–2699. b) C. K. Chang, I. Abdalmuhdi, *Angew. Chem.* **1984**, *96*, 154; *Angew. Chem. Int. Ed. Engl.* **1984**, *23*, 164–165. c) S. S. Eaton, G. Eaton, C. K. Chang, *J. Am. Chem. Soc.* **1985**, *107*, 3177–3184. d) C. A. Hunter, J. K. M. Sanders, A. J. Stone, *Chem. Phys.* **1989**, *133*, 395–404. e) Y. Le Mest, M. L'Her, N. H. Hendricks, K. Kim, J. P. Collman, *Inorg. Chem.* **1992**, *31*, 835–847.

[16] a) S. G. DiMagno, V. S.-Y. Lin, M. J. Therien, *J. Am. Chem. Soc.* **1993**, *115*, 2513–2515 . b) S. G. DiMagno, V. S.-Y. Lin, M. J. Therien, *J. Org. Chem.* **1993**, *58*, 5983–5993.

[17] A clear advantage of the porphyrin *meso*-aryl substituents is the prevention of aggregation of these chromophores in solution. The features observed in the electronic absorption or emission spectra remain invariant over a concentration range of 10^{-4} to 10^{-6} M; moreover, only a small bathochromic shift of these spectra is observed when axial ligands such as pyridine are added. The absorptive and emissive properties of these chromophores stand in sharp contrast to examples of butadiynyl-bridged porphyrins reported by Anderson, who has demonstrated that axial ligation is required to prevent association of conjugated porphyrin arrays derived from β-alkyl-substituted porphyrin building blocks (ref. [13b]).

[18] S. Priyadarshy, M. J. Therien, D. N. Beratan, unpublished results.

[19] M. J. S. Dewar, E. G. Zoebisch, E. F. Healy, J. J. P. Stewart, *J. Am. Chem. Soc.* **1985**, *107*, 3902–3909. For a recent reference in which MOPAC is utilized to determine optimized geometries in extended chromophore arrays, see: T. X. Lü, J. R. Reimers, M. J. Crossley, N. S. Hush, *J. Phys. Chem.* **1994**, *98*, 11878–11884.

[20] D. C. Miller, V. S.-Y. Lin, M. J. Therien, unpublished results.

[21] A point-dipole analysis of the optical spectra of these systems corroborates a picture in which the porphyrin–porphyrin geometrical relationships within the supermolecule are approximately coplanar (ref. [4]).

[22] M. Gouterman, in *The Porphyrins, Vol. III* (Ed.: D. Dolphin), Academic Press, London, **1978**, pp. 1–165.

[23] Excitation spectra for compounds **1**–**7** mirror their absorption spectra as expected from Kasha's rule, while compound **8** exhibits a diminished emissive signal at long wavelength.

[24] M. Kasha, H. R. Rawls, M. A. El-Bayoumi, *Pure Appl. Chem.* **1965**, *11*, 371–392.

[25] V. S.-Y. Lin, M. J. Therien, unpublished results.